

Ab initio studies of opto-electronic excitations in VO₂

Adam Gali^{(1,2)*} and John E. Coulter³ and Efstratios Manousakis^(3,4)

⁽¹⁾*Institute for Solid State Physics and Optics, Wigner Research Center for Physics,
Hungarian Academy of Sciences, Budapest, P.O.B. 49, H-1525*

⁽²⁾*Department of Atomic Physics, Budapest University of Technology
and Economics, Budafoki út 8., H-1111, Budapest, Hungary*

⁽³⁾*Department of Physics and National High Magnetic Field Laboratory,
Florida State University, Tallahassee, FL 32306-4350, USA*

⁽⁴⁾*Department of Physics, University of Athens, Panepistimioupolis, Zografos, 157 84 Athens, Greece.*

(Dated: October 23, 2018)

We study the optical response of VO₂ in the M1 insulating phase using methods based on density functional theory in its most recent developments. We start from a hybrid functional approach which may be a good starting point to carry out many-body perturbation theory since, as we show, it gives a qualitatively and to some degree quantitatively correct description of the insulating phase. In order to calculate the dielectric function, first, using hybrid density functional wavefunctions we have added GW corrections on top of the hybrid density functional calculations and we solved the so-called Bethe Salpeter equation to include effects of correlations of the electron-hole pair created upon photon absorption. We find that the effects of electron correlations are very important and they show up as a strong contribution of the electron-hole interaction in calculating the effects of the Bethe-Salpeter equation in the electron/hole pair excitation on top of the interacting group state.

I. INTRODUCTION

A plethora of fascinating new phenomena has been recently reported on oxide hetero-structures of transition metal oxides (TMO) and devices.¹⁻³ For example, an interface between two insulators behaves as a metal² which becomes superconducting at sufficiently low temperatures, while an interface between two antiferromagnets becomes ferromagnetic.⁴ These new structures not only create a playground for unexpected physical phenomena to be observed, but, in addition, they open up the possibility for new applications based on radically different foundations. Probing such interesting new phenomena is quite difficult due to impurity effects, lattice imperfections, and other materials-growth limitations. Very recent progress in material synthesis,^{1,3,5-9} however, is starting to make it possible to carefully investigate these fascinating systems.

The complex, unusual, and as yet not fully discovered or understood behavior of these strongly correlated materials, such as transition metal oxides (TMO), can be manipulated in a variety of fundamentally new applications. In particular, we would like to mention one such possibility which has been recently proposed¹⁰ by one of the authors of the present paper. This is based on the fact that these strongly correlated localized electrons form an electronic system which can be near the metal to Mott-insulator transition.¹¹ Photovoltaic devices based on carefully chosen doped Mott insulators can produce a significant photovoltaic effect. More importantly, it was found¹⁰ that if the Mott insulator is appropriately chosen, the photovoltaic effect can lead to solar cells of high efficiency, where a single solar photon can produce multiple electron/hole pairs, an effect known as impact ionization, in a time-scale shorter than the time charac-

terizing other relaxation processes. Increase of solar cell efficiency due to this process has been proposed previously for band-gap semiconductors; however, the effect is not significant there, because the characteristic time-scale for impact ionization is comparable to the time-scale for electron-phonon relaxation. The reason that this is not expected to hold for a Mott insulator is that the large Coulomb repulsion present in a Mott insulator leads to a large enhancement of the impact ionization rate.

It is very important to have a computational *ab initio* scheme which is reliable to evaluate opto-electronic properties such as excitations, gaps, absorption and, ideally to be able to compute the induced photo-current for a given bulk or interface structure. Furthermore, this scheme should be reliable for transition metal oxides where the electronic Coulomb correlations are expected to play an important role. Assuming that such a scheme exists, it would be very valuable in a variety of applications in real materials, including in the case of photovoltaic applications proposed in Ref. 10. This tool would meaningfully aid experimental efforts towards finding the most suitable TMO based material with suitable size gap, band structure, size of transition matrix elements including selection rules, etc.

In this paper we choose to study the optical properties of the insulating M1 phase of VO₂. Vanadium dioxide is regarded as the prototypical example of a strongly correlated TMO material with a long history starting with the original suggestion by Mott himself¹² and his collaborator Zylbersztein nearly four decades ago. Furthermore, this material has been the playground for almost all many-body techniques available to tackle strong Coulomb correlations.

VO₂ undergoes a structural distortion below approxi-

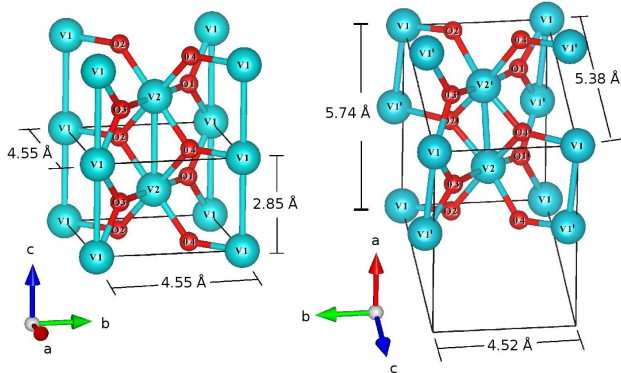


FIG. 1. (Color online) Unit cell of metallic and M1 phase of VO_2 single crystal. The symmetry axes of these crystals are shown. The rutile c -axis is applied as a “parallel” direction for the distorted M1 phase in the context which is conventionally called a -axis in M1 phase. The experimental lattice constants are also depicted.

mately $T_S \sim 340\text{K}$ at ambient pressure^{13,14}. Above T_S the structure of VO_2 is rutile-type and it is metallic and below T_S VO_2 is an insulator. The insulating low temperature phase is monoclinic and is called the M1 phase. We would like to focus our studies on this phase because it is an insulator that exists at room temperature which could be utilized for photovoltaic applications.

Below T_S and at room temperature, the vanadium (V) atoms dimerize and the V-V pair tilt around the rutile c -axis, doubling the unit cell as illustrated in Fig. 1. This dimerization causes a zigzag-like antiferroelectric tilt of the V atoms perpendicular to this axis. The dimerization affects mainly the V $3d t_{2g}$ states, which in the metallic phase fall near the Fermi energy and have similar band occupations.^{14,15} In the dimerized state, these states hybridize differently to form d_{\parallel} and π^* states. The bonding d_{\parallel} states fall below the π^* states, and they become fully occupied by the single d electron, leading to the insulating behavior due to this Peierls-type distortion. Our calculations support this picture and we illustrate what actually happens as the system undergoes the phase transition from the metallic to the insulating M1 phase in Sec. III C of this paper.

Previous *ab initio* calculations of optical properties, such as of the real and imaginary parts of the zero momentum dielectric function, show vast disagreement between the result of the calculation and the experimental results. For example, dielectric results from the local density approximation (LDA) within density functional theory (DFT)^{16,17} must be shifted entirely by hand to begin to agree with experiment.¹⁸ Results from a generalized gradient approximation of DFT (GGA) together with a Hubbard-correction,¹⁹ GGA+ U look strikingly different

apart from matching the optical gap²⁰ (which is effectively set by hand by tuning U). In addition, the electronic structure is predicted to be metallic rather than insulating using both LDA and GGA.^{21,22}

Methods that go beyond ground-state DFT are now well established. However one should remember that a better starting point is absolutely necessary for d -electrons.

With LDA+ U one gets antiferromagnetic insulating ground states for both the M1 and the metallic phase.²³ In addition, it treats differently the various orbitals and we do not always *a priori* know which orbitals need this special treatment. Furthermore the exact value of the parameter U is not known and it is phenomenologically determined.

The combination of LDA and dynamical mean-field theory (DMFT)^{24,25} has correctly described the M1 phase. However, a parameter free theory to describe correctly both the metallic and the insulating M1 phase is still absent.

The self-consistent COHSEX approximation of the GW-method²⁶ gives a good description of quasi-particle states and has been applied to VO_2 rather recently²⁷ with interesting results and conclusions. Furthermore, several authors have used *hybrid functionals*, a rather *ad hoc* procedure, and this approach seems to be a good compromise in many systems²⁸ including VO_2 .²¹ There is no good theoretical justification for the success of this procedure.

Optical absorption experiments create an interacting electron-hole pair, the exciton. Good agreement between theory and experiment can only be achieved by taking into account the exciton, especially if the system is a semiconductor or an insulator. Small-gap semiconductors and metals screen excitons. For accurate absorption spectra where such excitonic effects are important one has to solve the Bethe-Salpeter equation (BSE)²⁹ which uses the intuitive quasiparticle picture. The intrinsic two-particle nature of the BSE makes the calculations very cumbersome, since a four-point equation (due to the propagation of two particles) has to be solved.

In the present paper we go one step further in the characterization of the M1 phase of VO_2 crystal. The hybrid functional approach provides a better starting point, with the correct qualitative features, such as the correct symmetry of the ground state and a finite gap for a system in the insulating state; therefore, one expects that if we carry out many-body perturbation theory on top of a hybrid functional approach, such as HSE06,^{30,31} and we include the perturbative corrections, i.e., HSE06+GW and HSE06+GW+BSE, we will find a good convergence of the perturbative series.

In the following we describe our approach in the calculation of opto-electronic excitation of VO_2 in Section II. Here, we describe the applied density functionals and convergence tests on different parameters of the calculations. In the next sections we present our results and compare them to known experimental data. First, we

show the calculated electronic structure with different methods and compare them to photo-emission data in Section III. Here, we particularly analyze the phase transition from metallic rutile structure to the M1 Mott-semiconductor structure of VO₂. In addition, we validate a hybrid density functional with a parameter-free many-body perturbation theory method. Next, we describe the results on the optical properties of the M1 phase of VO₂ in Section IV, again, and compare them with the recorded absorption spectrum. Finally, we summarize and conclude our results in Section V.

II. THE APPROACH

We carried out DFT calculations on the M1 phase of VO₂ as implemented within the VASP package.³² We used small core projectors for vanadium ions, so we explicitly included 3s3p electrons as valence. The valence electron states were expressed as linear combination of plane waves. We found that the plane wave cutoff of 400 eV provided convergent single particle levels. We used the experimental geometry in all the calculations as shown in Fig. 1. We attempted to optimize the structure using the hybrid functional; the converged geometry disagrees with the experimental geometry rather significantly (the largest disagreement of the lattice constants was 3%), giving rise to a larger gap by a factor of 2 than that obtained by the same hybrid functional using the experimental geometry. We applied various numbers of k -points for the unit cell depending on the calculated properties. We found that the required size of the Monkhorst-Pack³³ k -point set depends strongly on the existence of a Mott gap. Namely, convergent charge density could be achieved already with a $5 \times 5 \times 5$ Monkhorst-Pack k -point set when there is a Mott-gap, while an $18 \times 18 \times 18$ k -point set was required when there was no Mott-gap. We show below that BSE calculations needed special treatment.

A. The general methodology

As a necessary step, first, we carry out standard LDA and GGA-type PBE³⁴ calculations for the ground state density of states (DOS), the band structure, and the optical response (the real and imaginary part of the dielectric function) of VO₂. Then, we carry out hybrid functional calculations, such as HSE06^{30,31} which involve using a much more computationally demanding computational scheme. The reason we begin from such calculations is that the standard LDA or GGA calculations give a single particle spectrum with significant density of states at the Fermi level (see Fig. 5) and no gap. This is a qualitatively different state from the correct ground state, and, thus, not suitable as a starting place for a perturbative scheme. The hybrid functionals, as we find, give a quasiparticle gap of the same order of magnitude as the observed gap, and thus, we can use them as a starting

point in a many-body perturbation theoretical approach to find the leading corrections.

The HSE functional for the exchange-correlation part of the energy involves a parameter a which mixes the contribution of the short-range parts of the Hartree-Fock exchange and the PBE expression for the exchange energy:³⁰

$$E_{xc} = aE_x^{HF,SR}(\omega) + (1-a)E_x^{PBE,SR}(\omega) + E_x^{PBE,LR}(\omega) + E_c^{PBE} \quad (1)$$

where the parameter ω defines what is meant by short and long ranged part of the Coulomb potential, which is split according to

$$\frac{1}{r} = \frac{\text{erfc}(\omega r)}{r} + \frac{\text{erf}(\omega r)}{r}, \quad (2)$$

where the part involving the complementary error-function $\text{erfc}(\omega r) = 1 - \text{erf}(\omega r)$ is the short-range and the part involving the error-function itself is the long-range part. The value of the parameter $\omega = 0.2a_0^{-1}$ is determined to give a balanced description that provides good accuracy and speed for both molecules and solids.³¹ The $E_x^{HF,SR}(\omega)$ is the Hartree-Fock exchange part which is calculated using the short-range part of the Coulomb interaction. $E_x^{PBE,SR/LR}(\omega)$ is the Perdew *et al.*³⁴ expression for the exchange energy functional which is modified to use the short/long range part of the Coulomb interaction.³⁰

The value of the mixing parameter $a = 1/4$ has been used in a variety of materials giving rather reasonably accurate values for the energy gap and other quasiparticle properties. Rationale for this functional and for the choice of this value for a is given in Ref. 35. There was argued that $a = 1/n$ with $n = 4$ should be the optimum choice for typical molecules for which fourth-order Møller-Plesset perturbation (MP4) yields atomization energies with a small mean absolute error. The case of $n \gg 4$ arises when there is a nearly-degenerate ground-state of an unperturbed problem which corresponds to the Kohn-Sham non-interacting system. An ideal hybrid should be sophisticated enough to optimize n for each system and property.³⁵ In the present paper, for the case of VO₂ we provide results for $n = 4$ and for $n = 8$. The former is the so-called HSE06³¹ functional, and the latter we will refer to in the following as HSE-1/8. We also refer to HSE06 in the following discussion as HSE-1/4 functional.

As a next step, we used the so-called G_0W_0 approximation to calculate the quasiparticle spectra, as implemented in VASP.³⁶⁻³⁹ This means that we have used in G_0 and W_0 the Kohn-Sham eigenvalues and orbitals. For W we take $W_0 = \epsilon^{-1}V$, where the dielectric matrix $\epsilon_{\mathbf{G},\mathbf{G}'}^{-1}(\mathbf{q},\omega)$, with \mathbf{G} and \mathbf{G}' denoting reciprocal lattice vectors, is calculated in the random phase approximation and the self-energy corrections are evaluated to first order in the difference between the self-energy Σ and the Kohn-Sham potential.⁴⁰ We note that we also carried out calculations where G was updated by n iterations

together with the DFT wave functions following the procedure described in Ref. 39. We denote this method by G_nW_0 .

In order to calculate the optical spectra,

a) as a first approximation, we use the independent particle approximation, i.e., using the energies and wavefunctions obtained in LDA, GGA, HSE-1/4 and HSE-1/8.

b) Then, we use the GW approximation on top of the HSE-1/4 and HSE-1/8 approximation. This corrects the quasiparticle properties, such as the density of the states. A small correction due to the GW relative to the starting point indicates that the starting level of approximation may be good.

c) However, transition metal oxides contain electrons near the Fermi level (in our case the the electrons occupying the Vanadium d -states) which are expected to be strongly correlated. This means that the electron-hole interactions are expected to be strong which should play a significant role in excitonic particle/hole states. These states are optically excited, therefore, we should and we will include the role of the particle/hole interaction in the calculation of the dielectric function. This is done using the Bethe Salpeter equation (BSE).²⁹

B. HSE-1/4 and HSE-1/8

In this subsection we discuss the results for the single particle DOS obtained with the two hybrid functionals HSE-1/4 and HSE-1/8 and their GW corrections. The DOS as a result of the GW calculation is obtained by finding the average energy shift (relative to the Fermi energy) for each quasiparticle energy level, and shifting the DOS calculated within DFT by the corresponding amount. This method is used due to the fact that a GW calculation with a really fine k -space mesh is extremely computationally expensive.

As can be observed in Fig. 2, the results for the DOS obtained using the HSE-1/4 (solid red line) functional and those obtained using the HSE-1/8 functional are different, especially for the Vanadium d -states just below the Fermi energy. The inclusion of the G_0W_0 corrections has a small effect on the results of the HSE-1/4 calculation and a much larger effect on the results obtained starting from the HSE-1/8 hybrid. Notice, however, that the final results, i.e., HSE-1/4+ G_0W_0 and HSE-1/8+ G_0W_0 are much closer to each other, especially for the deeper (relative to the Fermi energy) states, than the corresponding results without the G_0W_0 corrections.

In principle, if we were to carry out a perturbation series calculation to all orders on top of either HSE-1/4 or HSE-1/8, the final results should be the same. We have carried out higher order GW corrections, up to G_4W_0 , on top of both HSE-1/4 and HSE-1/8. As expected the results, obtained by iterating the GW four times on top of the HSE-1/8, which is illustrated in Fig. 2(bottom), show that the corrections beyond the G_0W_0 are small.

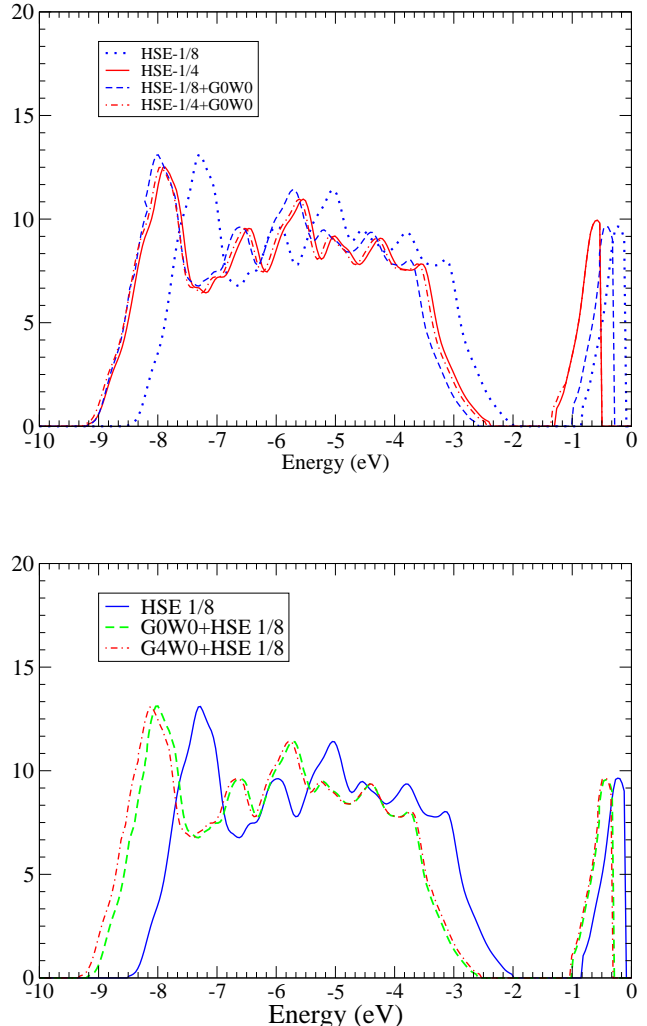


FIG. 2. (Color online) Top: Results for the density of states (DOS) obtained with HSE-1/4 (red solid line) and HSE-1/8 (blue dotted line) and with HSE-1/4+ G_0W_0 (red dot-dashed line) and HSE-1/8+ G_0W_0 (blue dashed line.) Bottom: Convergence study of the HSE-1/8+GW. The solid blue line is the result obtained with just HSE-1/8. The green dashed line is obtained by adding G_0W_0 to the HSE-1/8 and the red dot-dashed line is obtained after iterating GW for the 4th time starting from HSE-1/8.

Therefore, this leads us to conclude that the remaining difference between the HSE-1/8+GW and HSE-1/4+GW is not due to insufficient convergence of the GW iteration procedure. We think that this difference is due to processes not captured by the GW approximation. As we will demonstrate here by solving the BSE equation, the effects of the quasielectron-quasihole interaction are large. For example, the reason for the disagreement between HSE-1/8+GW and HSE-1/4+GW may be the fact that GW does not include the role of virtual two-particle/one-hole excitations. Furthermore, because the G_0W_0 corrections on top of the HSE-1/4 are smaller than the G_0W_0 corrections on top of the HSE-1/8, we may conclude that the HSE-1/4 provides a better starting point.

C. Convergence of BSE Calculations

The BSE calculation is computationally demanding because of the fact that one has to include the interaction of particle/hole pairs into different relative momenta and from different bands. As a result, to make the calculation feasible within realistic computational time scales, we need to limit the k -point size.

We have studied the convergence with respect to the size of k -point set used in our calculations. In Fig. 3 (top) we compare our calculated imaginary part of the dielectric function ϵ_2 parallel to the a-axis ($\epsilon_{2||}$) as calculated starting from the HSE-1/4 and adding the G_0W_0 correction and solving the BSE for a $5 \times 5 \times 5$ and a $7 \times 7 \times 7$ k -point set,³³ by including the same number of occupied and unoccupied bands in both calculations. All of our results are smoothed using an exponentially weighted moving average approach. This approach leads to the curves shown in Fig. 3 (bottom). Notice that the results of these two calculations agree reasonably well and, thus, we have adopted the $5 \times 5 \times 5$ k -point set in our calculations.

In Fig. 4 we demonstrate that using 26 occupied bands in our calculation maybe sufficient to achieve a satisfactory level of accuracy for $\epsilon_{2||}$. In all the calculations presented in Fig. 4, we have used 26 unoccupied bands ($NV = 26$) and we varied the number of occupied bands, namely, we used $NO = 12, 15, 20, 26, 36$. Notice that the results for $NO = 26$ have virtually converged, namely, these results are very close to those obtained for $NO = 36$. We have also studied the same convergence with respect to the number of the unoccupied bands by keeping the number of occupied bands fixed and found that when $NV = 26$, the results have converged. Therefore, all the results presented in this paper were obtained with $NO = NV = 26$.

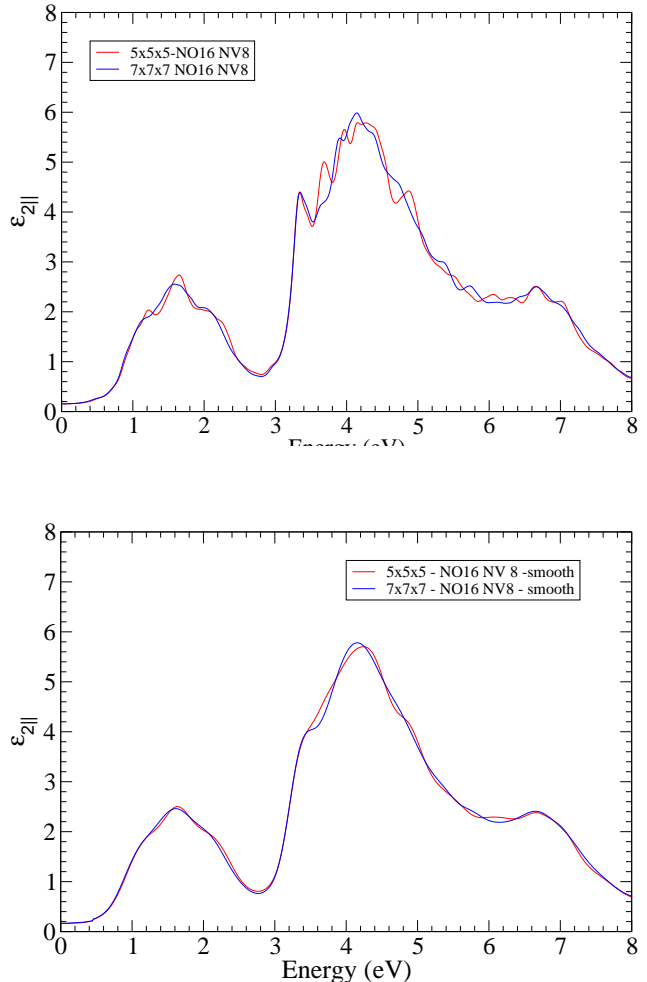


FIG. 3. (Color online) (Top) The parallel to the a-axis imaginary part of the dielectric function as calculated for a $5 \times 5 \times 5$ and a $7 \times 7 \times 7$ k -point set, by including the same number of occupied and unoccupied bands (18 occupied and 8 unoccupied). (Bottom) The data shown in the top part of this figure are smoothed using an exponentially weighted moving average technique. See Fig. 1 for the convention of parallel direction.

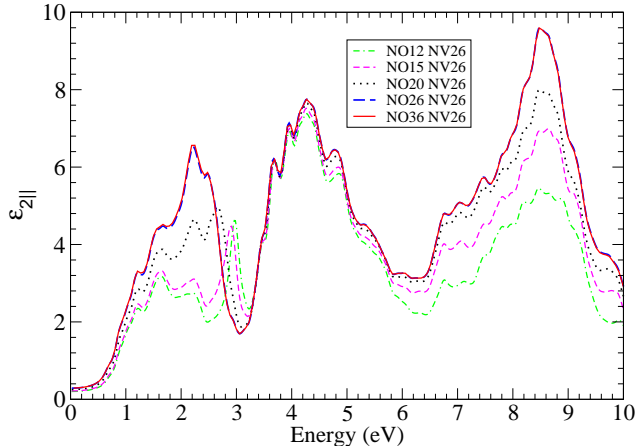


FIG. 4. (Color online) Convergence of $\epsilon_{2||}$ with number of occupied bands using a fixed number of unoccupied bands for the case of the full BSE calculation. See Fig. 1 for the convention of parallel direction.

III. DENSITY OF STATES

A. Comparison with photo-emission and band-structure

In this section we present and compare the results obtained with the various levels of approximation, namely, LDA, PBE, HSE, and HSE+GW. In addition, we will compare with the photo-emission experiments.

In Figs. 5, 6 we compare the density of states (DOS) as calculated using LDA, PBE, HSE-1/4 and HSE-1/8 with photoemission data.⁴¹ Notice that while the LDA and PBE calculations give a reasonably good account for the occupied states which are in the range of 2 eV to 8 eV below the Fermi level, both fail to describe the states which lie just below the Fermi level. On the contrary, it appears that the HSE-1/4 calculation gives a reasonable account of the density of states in this narrow region. This is a very interesting observation, which provides hope that a perturbative scheme involving the GW approach and the BSE starting from the HSE-1/4 wave functions might be a good idea.

B. Band Structure

This hope is also justified by comparing the results of the band structure, obtained with HSE-1/4 with those obtained by GW based calculations. In Fig. 7, the results of G_0W_0 calculation on top of HSE-1/4 (solid blue lines) are shown as red squares. In addition, we show the results of G_3W_0 calculation with black circles. The overall energy scale has been changed by a constant as

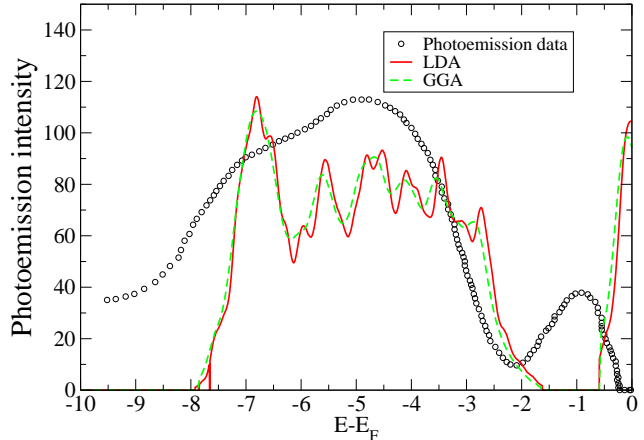


FIG. 5. The photoemission data taken from Ref. 41 is compared with the DOS of the occupied states as obtained from LDA, PBE calculations.

explained in the figure caption, in order for the Fermi levels to coincide. The overall small correction produced by GW indicates that the perturbative corrections on top of HSE-1/4 are small and, thus, we are hopeful that the perturbative series converges fast.

C. Partial density of states

In this subsection we discuss the changes that occur due to the phase transition from the metallic rutile phase to the insulating low temperature monoclinic M1 phase.

In Fig. 8 we present the calculated partial density of states projected around $V1$ and $O1$ (see Fig 1) for the rutile metallic phase (top) and the insulating M1 phase (bottom) near the Fermi level. If we choose different atoms, clearly, the contribution to the partial density of states of different orbitals will be changed according to the relative position of the other atom. Notice that the states with the largest weight crossing the Fermi energy in the metallic phase are of the t_{2g} symmetry. With our choice of axes (the x-axis is along the rutile c-axis, the y-axis is along a Vanadium-Oxide direction in one of the octahedra and the z-axis is along another Vanadium-Oxide direction in a different octahedron), the orbitals with t_{2g} symmetry are $d_{x^2-y^2}$, d_{yz} and d_{xy} , while the d_{z^2} and d_{xz} orbitals have e_g symmetry.

In the insulating phase, the states contributing the most in the total DOS just above the gap are mainly of the same t_{2g} symmetry. Just below the gap, however, only the $d_{x^2-y^2}$ orbital gives most of the contribution to the density of states. Namely, the dimerization of the V-V bond splits these t_{2g} states in opposite directions around the Fermi energy. The most affected orbital is

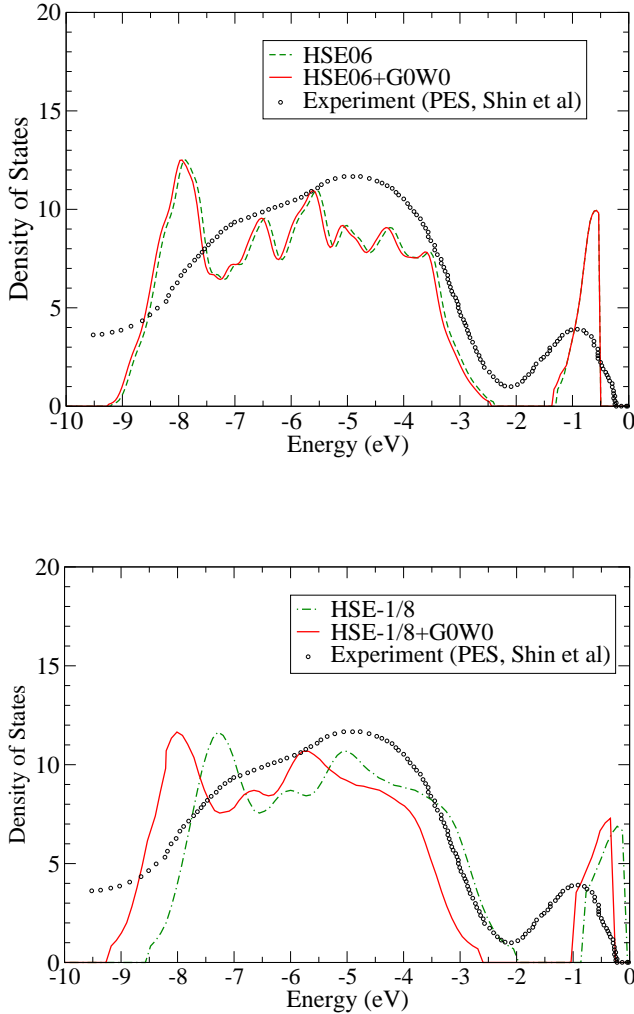


FIG. 6. The photoemission data taken from Ref. 41 is compared with the DOS of the occupied states as obtained from HSE-1/4 and HSE-1/4+ G_0W_0 (top) and HSE-1/8 and HSE-1/8+ G_0W_0 calculations. Notice that the band gap obtained is about 1.0 eV with HSE-1/4 and about 0.3 eV with HSE-1/8.

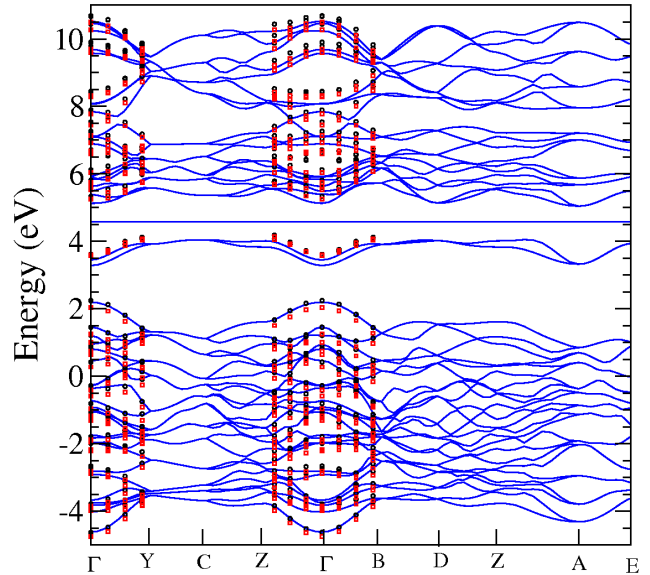


FIG. 7. (Color online) The band structure obtained with HSE-1/4 (Solid lines) is compared to that obtained by HSE-1/4+ G_0W_0 (red squares) and HSE-1/4+ G_3W_0 (black circles). The results of the GW calculations have been shifted downward by significant constant amounts, namely, the G_0W_0 calculation by 0.98 eV and the G_3W_0 calculation by 0.60 eV to make their Fermi energies (5.50 eV and 5.18 eV respectively) the same with the Fermi energy of the HSE-1/4 calculation (4.58 eV). Except for this overall constant, the bands from these calculations agree reasonably well with the HSE-1/4 calculation.

the bonding combination of the $d_{x^2-y^2}$ orbital, one lobe of which is directed along the V-V dimerization direction. Its energy is lowered relative to the Fermi level due to the dimerization. There is only one electron per V atom occupying these $d t_{2g}$ states which are near and below the Fermi energy. By entering the dimerized phase, where the unit cell doubles as shown in Fig. 1, each of the two pairs of $d_{x^2-y^2}$ orbitals (one from each of the four V atoms in the unit cell) form one bonding and one antibonding linear combinations which lead to two bonding and two antibonding bands. The energy of these two bonding bands is separated by a gap from the two antibonding bands and from the bands formed by all the other t_{2g} states. Thus, the four electrons which correspond to the two pairs of vanadium atoms which participate in the formation of the two bonding states, occupy and fill up all the states in the two bonding bands. These correspond to the two bands just below the Fermi level shown in Fig. 7. This gives rise to an insulating state with the rest of the t_{2g} states (along with the antibonding $d_{x^2-y^2}$ combinations) contributing to the bands just above the gap.

By inspecting Fig. 7, it becomes clear that these bands

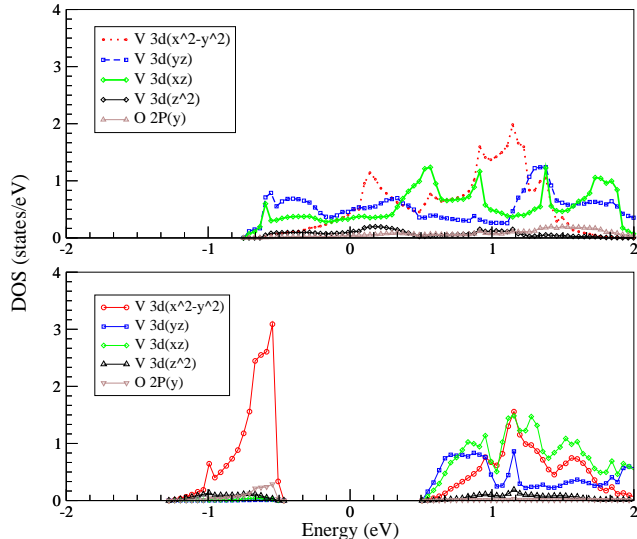


FIG. 8. The partial density of states near the Fermi level projected around $V1$ for a V state and around $O1$ for a O state (see Fig 1). Top: The rutile (metallic) phase. Bottom: The insulating (M1) low temperature phase. In both cases we have kept only the orbitals which contain more than 0.1 electrons (out of the 4 electrons total) below the Fermi level.

are more or less flat (a sign of one-dimensionality due to the directional character of the dimerization) except along two directions. The direction $\Gamma \rightarrow B$ and the direction $A \rightarrow E$. The former direction is along the dimerization direction (the a -axis in the M1 phase, see Fig. 1). The latter direction is along the b -axis of the M1 phase (Fig. 1). The former may be due to direct overlap of the $d_{x^2-y^2}$ orbitals along the a -axis, while the latter may be due to the hybridization of the $d_{x^2-y^2}$ with the oxygen p_y . We find that the $V1$ and $V2$ atoms connected to $O1$ have approximately the same distance from $O1$ and the line that begins from $O1$ and bisects the $V1 - V2$ line-segment is our y -axis. As a result, we should expect to find the overlap between the p_z (and the p_x) orbital of the $O1$ atom and the sum of the $d_{x^2-y^2}$ orbitals of the $V1$, and $V2$ atoms to should be small. This is what we see in Fig. 8, where the most significant contribution to the PDOS just below the gap in the M1 phase is due to $V d_{x^2-y^2}$ and the $O p_y$. This is not the case for the $O1'$ atom; in this case the $V1$ and $V2$ atoms connected to $O1'$ are not equidistant from $O1'$ due to the dimerization. As a result, the PDOS for atom $O1'$ shows contributions from p_x and p_y orbitals.

IV. DIELECTRIC FUNCTIONS

Here we present our calculated imaginary part of the dielectric function for momentum $q = 0$, as a function of frequency (energy) for light polarization parallel and perpendicular to the c -axis of the crystal. This physical quantity is directly accessible by optical studies.⁴²

In order to calculate the dielectric function, which for zero momentum transfer is directly proportional to the optical response, we will first work within the independent particle approximation. In this case the dielectric function is calculated using the energy eigenvalues and eigenvectors as obtained by LDA or PBE or HSE and the non-interacting “bubble-diagram” for the response function.

In Fig. 9 the $q = 0$ dielectric function as calculated using LDA and PBE is compared to the experimental results. Notice that while the higher energy peak is in reasonable agreement with the experiment, this calculation misses entirely the lower energy peak near ~ 1 eV and the overall distribution of strength of the response function.

The electron-electron interaction, however, affects the excited electron-hole pair, and it can create excitonic effects. In the simplest extension, we can take into account these interaction effects by solving the Bethe-Salpeter equation.²⁹ In doing so, the two-particle nature of the the BSE equation, makes the calculation cumbersome, because the four point Green’s function has to be solved self-consistently. This calculation requires very large memory, especially when one tries to include many occupied and unoccupied bands and a larger k -point set, and a lot of CPU time.

We found that the first allowed transition appears at about ~ 0.4 eV and ~ 0.2 eV for HSE-1/4+GW+BSE and HSE-1/8+GW+BSE methods, respectively, which can be tentatively compared to the calculated single particle gaps of 1.0 eV and 0.4 eV. This is a very large reduction (particularly for the HSE-1/4 functional) which implies strong electron-hole interactions. We emphasize here that very deep occupied states could seriously influence this value indicating the strong correlation between the holes and electrons. It may be suspected that this extremely large electron-hole interaction may be not well accounted for by the perturbative BSE approximation in this case. In the top of Fig. 10 the results for the imaginary part of the dielectric function $\epsilon(q = 0, \omega)$ for polarization parallel to the crystalline a -axis are presented for the two cases where (a) the HSE-1/4 and HSE-1/4+GW+BSE and (b) HSE-1/8 and HSE-1/8+GW+BSE are implemented and they are compared with the experimental data.⁴² In the bottom of Fig. 10 we present the results of the same calculations for the case of polarization perpendicular to the a -axis. Notice that the calculations based on the HSE-1/4 functional show two main peaks at approximately 2 eV and 4 eV which correspond to the experimental peaks at approximately 1 eV and 3 eV. Therefore, if the results of the full

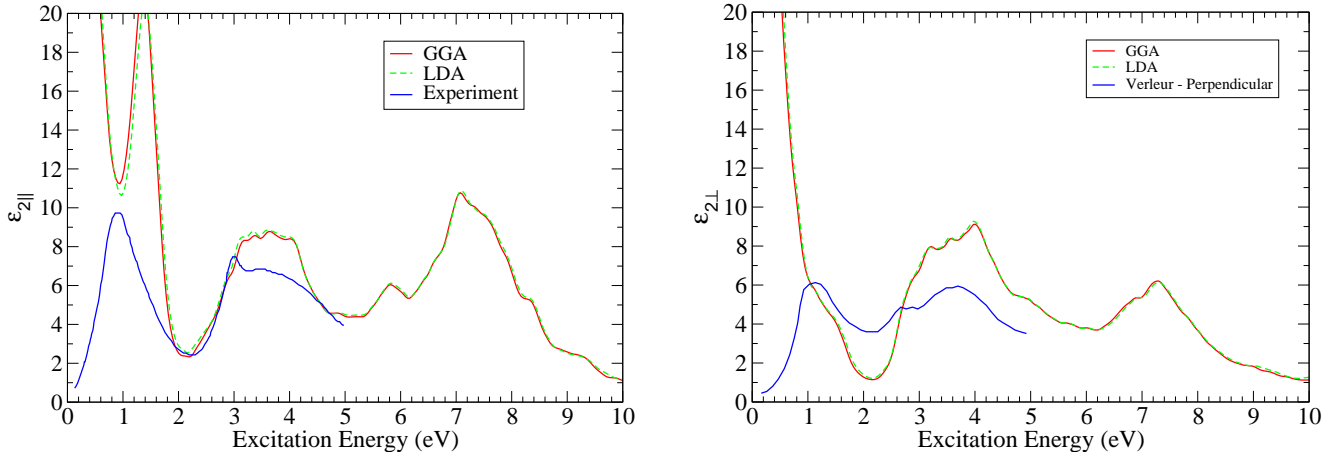


FIG. 9. (Color online) The experimental data taken from Ref. 42 for the imaginary part of the dielectric function at zero momentum as a function of frequency for the cases of polarization parallel (left) and perpendicular (right) to the a -axis is compared with the results of LDA and PBE. See Fig. 1 for the convention of parallel direction.

HSE-1/4+ G_0W_0 +BSE are shifted by a uniform amount of about 1 eV at lower energy they would agree with the experimental position of the peaks. The main reason for this disagreement arises from the HSE-1/4 calculation which overestimates the position of these peaks by approximately the same amount. Notice, however, that the BSE calculation brings the intensity of these peaks down to be comparable with the experimental intensity. Now, the results (right parts of Fig. 10) obtained by reducing the mixing parameter a in these calculations from its value of $a = 1/4$ in the HSE-1/4 functional to $a = 1/8$, show a better agreement with the experimental results. This may be a fortuitous coincidence since HSE-1/4 provides more accurate quasi-particle energies as confirmed by GW calculations. In HSE-1/8 functional the wavefunctions are less localized than by HSE-1/4 functional which enter BSE equations. That might compensate the neglect of the role of the electron-phonon interaction in the imaginary part of dielectric function. Furthermore, since we found that the electron-hole interaction has a large effect on the dielectric function $\epsilon(\omega)$, one would need to include self-energy corrections due to two-particle+one-hole intermediate states.

A. Optical Transitions

It is important to note that the nature of the optical transitions agrees well with previous analysis of the behaviour of this material^{21,41}, as the exact nature of these transitions has been in question for some time. By comparing the optical spectra (Fig. 10) to the expanded PDOS in Fig.11, we can see quite clearly the transitions occurring at each peak in the spectra. It seems safe to

do so using the projected density of states within the HSE-1/4 picture, as the BSE calculation did not largely shift the position of the peaks in the optical spectra, but only modulated the intensity of the quasiparticle energies. The first peak in the optical spectra is entirely due to the excitation of the filled t_{2g} states to the un-filled anti-bonding t_{2g} states. No other transitions at this energy range are possible. At photon energies of $\sim 3eV$, the transition from filled $O 2p$ states to the same anti-bonding t_{2g} states becomes available. The transition from the filled valence band to the higher-energy $V 3d(e_g)$ anti-bonding states becomes available at about $4eV$, adding to the height of the 2nd peak. The third peak at around $8eV$ arises from the transition between $O 2p$ states and the anti-bonding $V e_g$ states.

V. SUMMARY AND CONCLUSIONS

We computed the ground state and optical properties of the M1 phase of the VO_2 single crystal by means of density functional theory and beyond. We found that the HSE-1/4, i.e., the HSE06 functional provides a better description to the single particle levels as inferred from quasi-particle correction within GW approximation. However, the calculated gap is about 1.0 eV which is about 0.6 eV larger than gap inferred by room-temperature photoemission measurements. We suspect that the neglected vertex corrections in the quasi-particle correction and/or the electron-phonon interaction are responsible for this discrepancy.

In agreement with prior work, we find that the transition to the M1 phase causes a Peierls-like distortion which, out of the three bands of t_{2g} symmetry, it affects

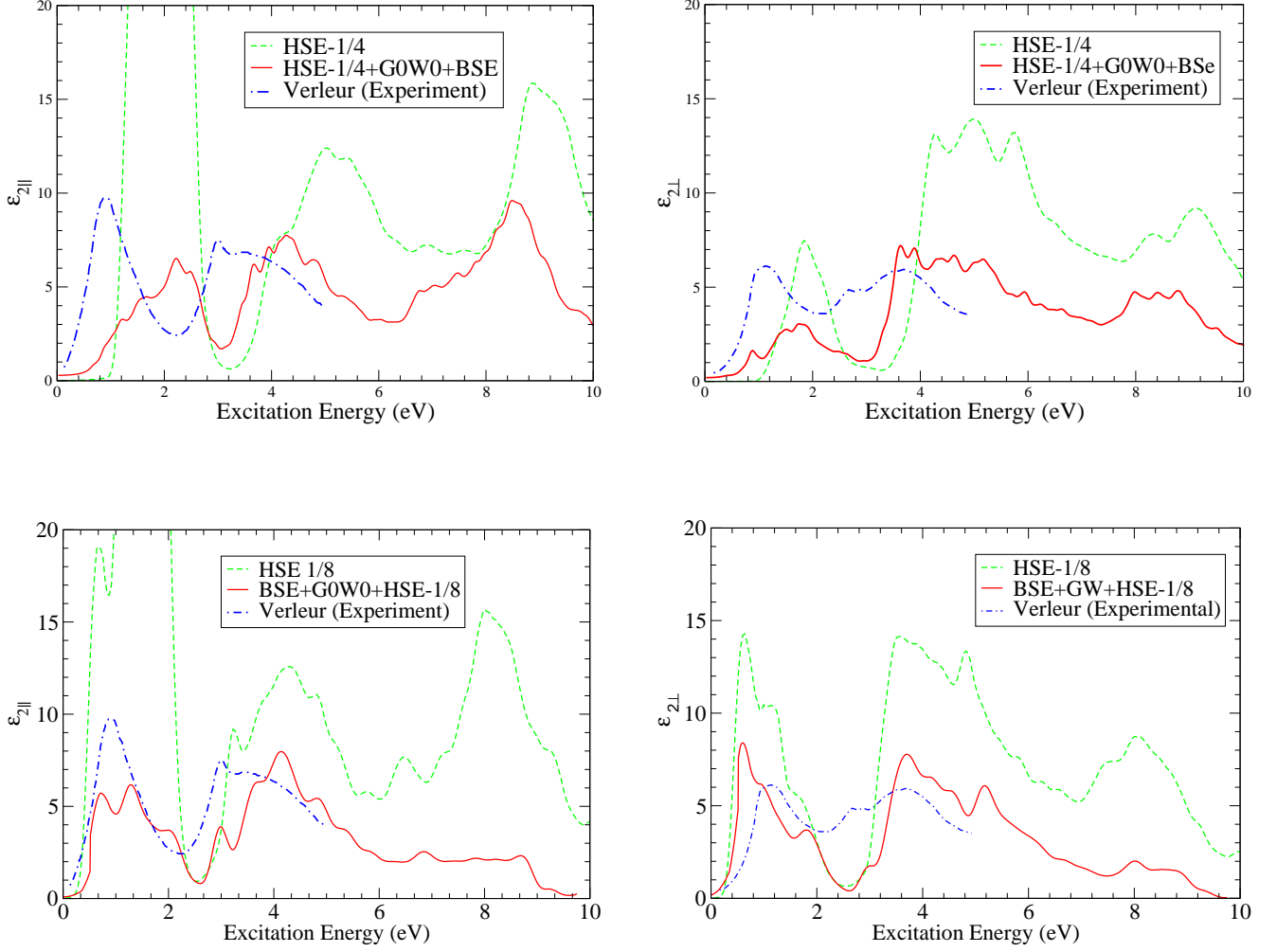


FIG. 10. (Color online) The experimental data taken from Ref. 42 for the imaginary part of the dielectric function for polarization parallel (left column) and perpendicular (right column) to the a-axis at zero momentum as a function of frequency, is compared with the results of HSE-1/4 and HSE-1/4+GW+BSE (top row) and with the results of the HSE1/8 and HSE1/8+GW+BSE (bottom row). See Fig. 1 for the convention of parallel direction.

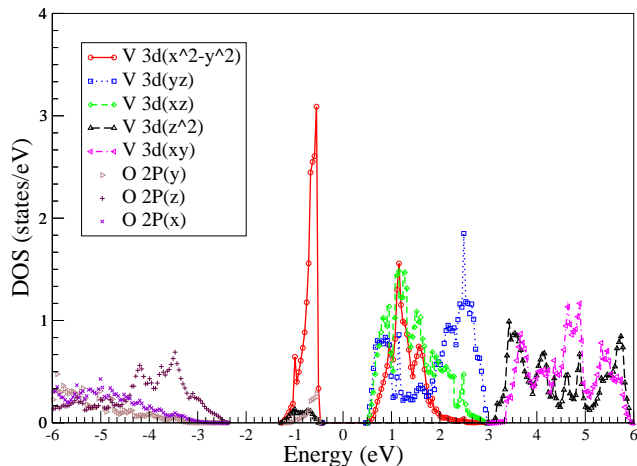


FIG. 11. (Color online) The PDOS projected as in Fig. 8, expanded to show the nature of transitions observed in the optical spectra. As before, states with small contribution are removed from the plot for clarity.

the band which is mainly of V $d_{x^2-y^2}$ character. The four V atoms in the doubled unit cell after dimerization become two pairs and their corresponding four $d_{x^2-y^2}$ states lead to two bonding and two antibonding combinations separated by the Peierls gap. There are four electrons available for these bands and after the dimerization, the two bonding bands just below the Fermi energy become fully occupied, which leads to a Peierls insulator (for details see our Sec. III C).

A major new finding in our paper is that the electron-hole interaction in these oxide materials is very strong which leads to significant reduction of the overall response function relative to the starting hybrid functional results. We believe that this may be due to the pronounced localized nature of the $d_{x^2-y^2}$ orbital and the strong electron correlation arising from the charge localization. Occupied electron states with energy 10 eV below the Fermi-level have *substantial* effect on the calculated first absorption peak (~ 0.4 eV). This gives us hope that the screened Coulomb interaction between electrons and holes, which is strong in the M1 phase of

VO₂, might cause a high impact ionization rate, leading to multi-exciton generation upon high-energy excitation. We believe that this finding could be rather general among TMOs where the same interaction is responsible for the Mott-gap in this class of materials. Thus, Mott-insulators could indeed be an important class of materials of interest for photovoltaic applications. In addition to opto-electronic excitations, doping and extraction of carriers should be addressed in future studies in order to fully explore the applicability of this class of materials in third generation solar cells.

On the other hand, our results imply that it is very difficult to provide quantitatively accurate predictions for the optical response in the complex materials such as the M1 phase of VO₂, even by means of very sophisticated methods involving many-body perturbation theory. The disagreement with the experiment on the location of the two main (low energy) peaks in the imaginary part of the dielectric function might be attributed to the fact that we have neglected vertex corrections and the contribution of two-particle-one hole states in the quasiparticle self-energy, the electron-phonon interaction. Furthermore, it might be significant the contribution to the response function from three-particle three-hole states in this strongly correlated material which is obviously not captured by BSE. Nevertheless, the HSE06+G₀W₀+BSE results on the optical response in the energy region important for photo-voltaic applications, show a very large improvement relative to that obtained by independent particle approximations where the intensity of the response function by HSE06+G₀W₀+BSE is in good agreement with the experiments. This finding indicates that HSE06+G₀W₀+BSE method can be applied to semi-quantitatively predict optical excitations in transition metal oxides.

VI. ACKNOWLEDGMENTS

This work was supported in part by the U.S. National High Magnetic Field Laboratory which is partially funded by the U.S. National Science Foundation.

* agali@eik.bme.hu

¹ J. Mannhart and D. G. Schlom, *Science* **327**, 1607 (2010)
² C. Cen, S. Thiel, G. Hammerl, C. W. Schneider, K. E. Andersen, C. S. Hellberg, J. Mannhart, and J. Levy, *Nature Materials* **7**, 298 (2008)
³ A. Gozar, G. Logvenov, L. F. Kourkoutis, A. T. Bollinger, L. A. Giannuzzi, D. A. Muller, and I. Bozovic, *Nature Materials* **455**, 782 (2008)
⁴ S. Okamoto and A. J. Millis, *Nature* **428**, 630 (2004), (and references therein)
⁵ A. Bhattacharya, S. J. May, S. G. E. te Velthuis, M. Warusawithana, X. Zhai, B. Jiang, J.-M. Zuo, M. R. Fitzsim-

mons, S. D. Bader, and J. N. Eckstein, *Phys. Rev. Lett.* **100**, 257203(1) (2008)

⁶ C. Adamo, X. Ke, P. Schiffer, A. Soukiassian, M. Warusawithana, L. Maritato, and D. G. Schlom, *Appl. Phys. Lett.* **92**, 112508 (2008)

⁷ A. Bhattacharya, X. Zhai, M. Warusawithana, J. N. Eckstein, and S. D. Bader, *Appl. Phys. Lett.* **90**, 222503(1) (2007)

⁸ M. P. Warusawithana, E. V. Colla, J. N. Eckstein, and M. B. Weissman, *Phys. Rev. Lett.* **90**, 036802(1) (2003)

⁹ e. a. M. Warusawithana, *Science* **324**, 367 (2009)

¹⁰ E. Manousakis, *Phys. Rev. B* **82**, 125109 (2010)

- ¹¹ N. F. Mott, Proceedings of the Physical Society of London Series A **62**, 416 (1949)
- ¹² A. Zylbersztejn and N. F. Mott, Phys. Rev. B **11**, 4383 (1975)
- ¹³ G. Andersson, Acta Chem. Scand. **8**, 1599 (1954)**10**, 623 (1956)
- ¹⁴ J. B. Goodenough, Phys. Rev. **117**, 1442 (1960)
- ¹⁵ J. B. Goodenough, J. Solid State Chem. **3**, 490 (1971)
- ¹⁶ D. M. Ceperley and B. J. Alder, Phys. Rev. Lett. **45**, 566 (Aug 1980)
- ¹⁷ J. P. Perdew and A. Zunger, Phys. Rev. B **23**, 5048 (May 1981)
- ¹⁸ R. J. O. Mossaneck and M. Abbate, Journal of Physics: Condensed Matter **19**, 346225 (2007)
- ¹⁹ J. Hubbard, Proceedings of the Royal Society of London. Series A. Mathematical and Physical Sciences **276**, 238 (1963)
- ²⁰ G.-H. Liu, X.-Y. Deng, and R. Wen, Journal of Materials Science **45**, 3270 (2010), ISSN 0022-2461, 10.1007/s10853-010-4338-2
- ²¹ V. Eyert, Ann. Phys. (Leipzig) **11**, 650 (2002)Phys. Rev. Lett. **107**, 016401 (2011)
- ²² R. M. Wentzcovitch, W. W. Schulz, and P. B. Allen, Phys. Rev. Lett. **72**, 3389 (1994)**73**, 3043 (1994)
- ²³ M. A. Korotin, N. A. Shorikov, and V. I. Anisimov, Phys. Met. Metallogr. **94**, 17 (2002)
- ²⁴ S. Biermann, A. Poteryaev, A. I. Lichtenstein, and A. Georges, Phys. Rev. Lett. **94**, 026404 (2005)
- ²⁵ J. M. Tomczak and S. Biermann, J. Phys. Condens. Matter **19**, 365206 (2007)
- ²⁶ L. Hedin, Phys. Rev. **139**, A796 (Aug 1965)
- ²⁷ M. Gatti, F. Bruneval, V. Olevano, and L. Reining, Phys. Rev. Lett. **99**, 266402 (2007)
- ²⁸ V. L. Chevrier, S. P. Ong, R. Armiento, M. K. Y. Chan, and G. Ceder, Phys. Rev. B **82**, 075122 (2010), see Supplementary material.
- ²⁹ E. E. Salpeter and H. A. Bethe, Phys. Rev. **84**, 1232 (1951)
- ³⁰ J. Heyd, G. E. Scuseria, and M. Ernzerhof, J. Chem. Phys. **118**, 8207 (2003)
- ³¹ A. F. Izmaylov, A. V. Krukau, O. A. Vydrov, and G. E. Scuseria, J. Chem. Phys. **125**, 224106 (2006)
- ³² vienna Ab Initio Simulation Package (VASP) Version 5.2.2.G. Kresse and J. Furthmüller, Phys. Rev. B **54**, 11169 (1996)Comput. Mater. Sci. **6**, 15 (1996)
- ³³ H. J. Monkhorst and J. D. Pack, Phys. Rev. B **13**, 5188 (Jun 1976)
- ³⁴ J. P. Perdew, K. Burke, and M. Ernzerhof, Phys. Rev. Lett. **77**, 3865 (1996)
- ³⁵ J. P. Perdew, M. Ernzerhof, and K. Burke, J. Chem. Phys. **105**, 9982 (1996)
- ³⁶ M. Shishkin and G. Kresse, Phys. Rev. B **74**, 035101 (Jul 2006)
- ³⁷ M. Shishkin and G. Kresse, Phys. Rev. B **75**, 235102 (Jun 2007)
- ³⁸ F. Fuchs, J. Furthmüller, F. Bechstedt, M. Shishkin, and G. Kresse, Phys. Rev. B **76**, 115109 (Sep 2007)
- ³⁹ M. Shishkin, M. Marsman, and G. Kresse, Phys. Rev. Lett. **99**, 246403 (Dec 2007)
- ⁴⁰ M. S. Hyberstein and S. G. Louie, Phys. Rev. Lett. **55**, 1418 (1985)R. W. Godby, M. Schlüter, and L. J. Sham, **56**, 2415 (1986)
- ⁴¹ S. Shin, S. Suga, M. Taniguchi, M. Fujisawa, H. Kanzaki, A. Fujimori, H. Daimon, Y. Ueda, K. Kosuge, and S. Kachi, Phys. Rev. B **41**, 4993 (1990)
- ⁴² H. W. Verleur, J. A. S. Barker, and C. N. Berglund, Phys. Rev. **172**, 788 (1968)